THE JOURNAL OF PHYSICAL CHEMISTRY B

ARTICLE

pubs.acs.org/JPCB

Symmetric and Asymmetric Bolaamphiphiles from Ascorbic Acid

Christian Dolle,[†] Pietro Magrone,[‡] Sergio Riva,[‡] Moira Ambrosi,[§] Emiliano Fratini,[§] Niccolò Peruzzi,[§] and Pierandrea Lo Nostro*[,§]

[†]Ipf Leibniz-Institut für Polymerforschung Dresden e.V., 01069 Dresden, Germany

[‡]Istituto di Chimica del Riconoscimento Molecolare, Consiglio Nazionale delle Ricerche, 20131 Milano, Italy

[§]Department of Chemistry and CSGI, University of Florence, 50019 Sesto Fiorentino (Firenze), Italy

Supporting Information

ABSTRACT: The properties of novel bolaamphiphiles that carry epimers of vitamin C (L-ascorbic acid and/or D-isoascorbic acid) as hydrophilic head groups, and an interconnecting aliphatic C_{12} chain (DD, DL, and LL) were investigated by differential scanning calorimetry (DSC), thermogravimetric analysis (TGA), small-angle X-ray scattering (SAXS), X-ray diffraction (XRD), and Fourier transform infrared spectroscopy (FTIR) in the solid state (anhydrous powders) and in aqueous dispersions as a function of the surfactant concentration. Upon heating, the aqueous dispersions undergo a phase transition from a hydrated semicrystalline "coagel" to a micellar phase. The results suggest that the headgroup chirality determines the formation of either inter- or intramolecular hydrogen bonds between the polar heads, which affect the phase behavior and structural properties of the nanoassemblies produced by these surfactants in water dispersions. The DSC data of aqueous dispersions were analyzed to obtain the size distribution of the pores in the coagel state.

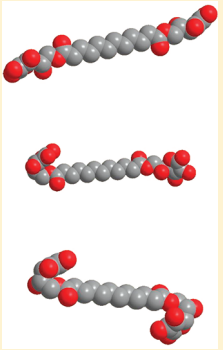

INTRODUCTION

Chirality is a key feature in chemistry and biosciences. In terms of structural hierarchy, its effects span from the molecular level (amino acids and sugars) up to the supramolecular level (nucleic acids, polypeptides, single cells, sea shells, and so on).[1−5] The relevance of this feature emerges in phenomena such as molecular recognition and functionalities of biological processes in living organisms.

Molecular chirality mainly derives from the asymmetry of chemical groups covalently bound to a central atom. In this case, chirality is permanent, as long as the bonds are not broken or unless a rearrangement of the mutual positions of the groups takes place. By contrast, supramolecular chirality derives from the nonsymmetric arrangement of molecular components in a noncovalent ensemble.[6,7] In these systems, constructed by molecular building blocks, the stability and the supramolecular structure result from the interplay of noncovalent interactions, e.g., van der Waals, dipolar, hydrophobic, electrostatic, $\pi-\pi$ interactions, hydrogen bonds, stacking, steric, and hydration forces. Such interactions are not permanent, but can be destroyed and reformed as a result of thermal, osmotic, or mechanical stress, pH changes, and so on.[8−12]

Surfactants spontaneously self-associate in water, producing a wide variety of supramolecular assemblies. If they bear stereogenic centers in their polar head groups they become a suitable tool for investigating the effect of stereochemistry on the shape, size, and other properties of self-assembled nanosystems.

Among the chiral surfactants, the amphiphilic derivatives of ascorbic acid are particularly interesting. In fact, they possess two stereogenic centers (carbons C-4 and C-5 of the ring), a quite rigid almost planar lactone ring, a flexible side chain, a redox active unit (the HO−C═C−OH group), and several oxygen atoms that can be involved as donors and/or acceptors in hydrogen bonding.

In previous contributions, we reported on the self-assembly properties of D-(−)-isoascorbyl-alkanoates (D-ASCn) in aqueous dispersions, as compared to those of the L-(+)-ascorbyl-alkanoates (L-ASCn) with the same chain length.[13,14] D-(−)-isoascorbic acid is an epimer of L-(+)-ascorbic acid, with a configuration inversion at C-5 (see Figure 1).

Although these molecules have the same reducing activity, the D-epimer possesses only 5% of the biological activity of L-ascorbic acid.[13,14] This difference has been attributed to the different hydration properties of the two species, and to the different perturbation they induce in the dynamical structure of bulk water.[15−18]

We found that the change in the C-5 stereogenic atom between the two isomers results in a different set of inter- and intramolecular hydrogen bonding interactions in the solid state and in a different hydration in aqueous dispersions of single-chained surfactants that bear either a D-ASCn or an L-ASCn polar head.[13,14]

When these amphiphiles are dispersed in water, they form hydrated crystalline phases (*coagels*) that turn into micellar

Received: May 26, 2011
Revised: August 31, 2011
Published: September 06, 2011

dispersions or gels upon heating, depending on the alkyl chain length.[19−21] In the literature, coagels are also described as "opaque suspensions of crystals", "poorly hydrated multilamellar polycrystalline suspensions", "hydrated solids" or "biphasic mixtures containing crystals".[22]

The coagel structure comprises a tight packing of interdigitated, nontilted, surfactant molecules arranged in lamellae with a thin interlayer of strongly bound water molecules, of about 10 Å. Macroscopically, the coagel is a turbid, highly viscous material that does not flow when the vial is turned upside down. In the so-called "gel", the hydrocarbon chains are in a partially molten state, and the structure is less crystalline, resulting in an almost transparent, viscous phase. In the gel, the aqueous interlamellar pool becomes wider (up to 100 nm) and comprises a layer of water molecules whose dynamic properties and mobility are intermediate between those of the strongly bound water and of the free bulk solvent.[23]

In a previous study, we investigated the nanostructures formed by a bolaform amphiphile, that bears two L-ascorbic acid moieties and one single hydrophobic chain (see Figure 2).[24] The results showed that in the coagel state the surfactant forms hollow monodisperse nanotubes, which turn into a clear micellar dispersion upon heating.

With these premises, in the present work we investigated the effect of chirality of the head groups on the self-assembly behavior of two bolaform surfactants carrying either two D-isoascorbic acid units (symmetric bolaamphiphile, DD) or one L- and one D- headgroup (asymmetric compound, DL) (Figure 3). The syntheses of these compounds were performed by exploiting the regioselectivity of lipases, thus avoiding coumbersome protective and deprotective steps. The results are compared to those obtained with the LL bolaamphiphile, and discussed in terms of the different inter- and intramolecular hydrogen bonds formed by the chiral head groups.

Moreover, in this work we investigated the different kinds of water molecules comprised in the aqueous dispersion. The first hydration layer of interfacial water contains molecules that are strongly bound to the surfactant hydrophilic groups, and do not melt during a differential scanning calorimetry (DSC) heating scan. The second type is bulk water with its normal dynamic and thermal properties. The third fraction of solvent molecules is confined in the micropores formed by the lamellar domains and possess a different thermal behavior. In particular, they have a reduced freedom of motion and are confined in cavities with nonzero curvature. Furthermore, if the micropores are in contact with the surrounding bulk solvent (as in the coagel),

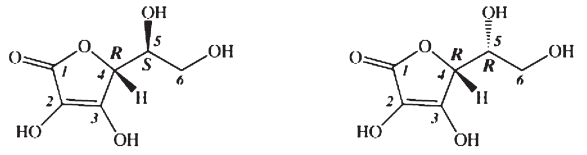

Figure 1. Chemical structure of L-(+)-ascorbic acid (left) and D-(-)-isoascorbic acid (right).

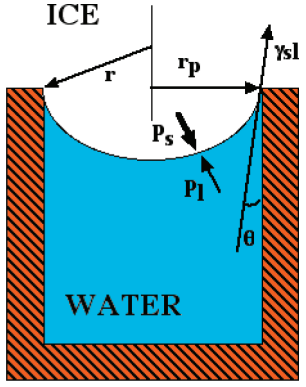

Figure 3. A small pool of water is confined within the pore and is in equilibrium with the ice above. Adapted from ref 25. Copyright 2005, with permission from Elsevier.

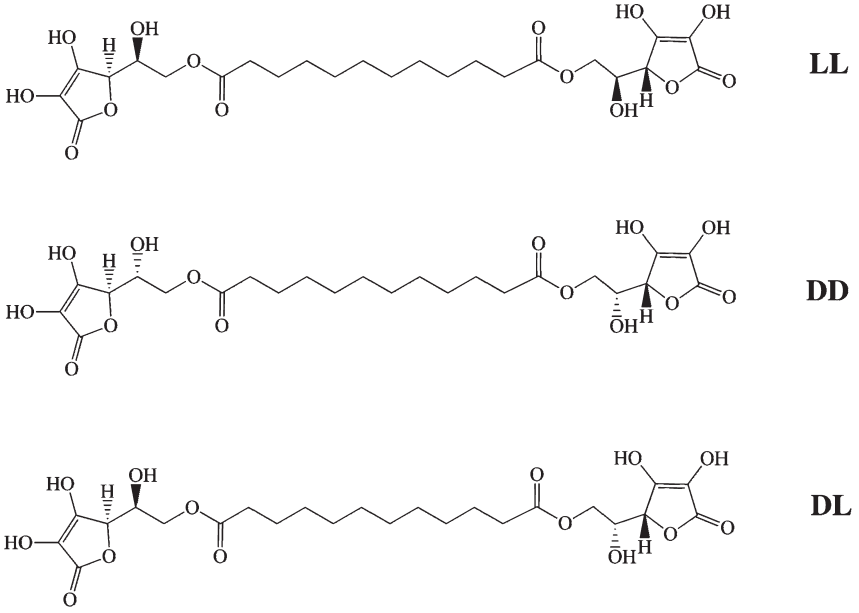

Figure 2. Chemical structures of LL, DD, and DL bolaform amphiphiles.

dx.doi.org/10.1021/jp204920y |J. Phys. Chem. B 2011, 115, 11638–11649

a new interface between the confined and the bulk water molecules will be created. For soft samples, such as those investigated in the present work, the pore size and distribution can be studied through small-angle X-ray scattering (SAXS), NMR, cryology, and DSC.[24] We adopted the procedure reported by Landry[25] to determine the pore size and their distribution in the coagel samples from the DSC data. To our best knowledge, this is the first time that thermoporometry has been used to describe the different kinds of water that are present in a coagel phase.

MATERIALS AND METHODS

All chemicals were obtained from commercial sources (Aldrich) and used without further purification. All solvents were of reagent grade or HPLC grade. Novozym435 (immobilized lipase from *Candida antarctica*) was a gift from Novozymes, Inc. Thin-layer chromatography (TLC) analysis were performed on precoated silica gel 60 F_{254} plates (Merck) and treated with the molybdate reagent ($(NH_4)_6MoO_{24}\cdot 4H_2O$, 42 g; $Ce(SO_4)_2$, 2 g; H_2SO_4 concentrated 62 mL; made up to 1 L with deionizated water) or $KMnO_4$ (0.5 g in 100 mL of NaOH 1 M) or UV light (254 and 366 nm). Flash chromatography was performed using silica gel 60 (70−230 mesh, Merck). Molecular sieves (4 Å, beads, 8−12 mesh) were preactivated at ca. 150 °C for 3 days. The ^{1}H NMR and ^{13}C NMR spectra were recorded at the specified field strength and in the solvent indicated using standard pulse techniques on Bruker 300, 400, or 500 MHz and Varian Mercury 300 MHz spectrometers at ambient temperatures. Chemical shifts (δ) were expressed in parts per million (ppm) and were referenced to TMS or the residual solvent peak. Coupling constants (J) are quoted to the nearest 0.1 Hz (Hz). Assignments of signals were made where possible, using COSY, DEPT, APT, HMQC, and HMBC experiments where necessary. Electron impact (EI) and fast atom bombardment (FAB) mass spectra were recorded at an ionizing voltage of 6 keV on a VG 70−70 EQ instrument.

6-*O*-[(+)-L-Ascorbic acid]-6′-*O*-[(+)-L-ascorbic acid] Dodecanedioate. To a solution of (+)-L-ascorbic acid (1.56 g, 8.87 mmol) and divinyl dodecanedioate (500 mg, 1.77 mmol) in acetone (30 mL), 4 Å molecular sieves (3 g) and Novozym435 (375 mg) were added. The suspension was kept at 45 °C and shaken at 250 rpm for 16 h. The reaction was monitored by TLC [EtOAc/MeOH/H_2O (8:2:0.3)] and terminated by filtering off the enzyme. The filtrate was evaporated under reduced pressur, and the residue was dissolved in water and extracted by EtOAc (3 × 50 mL). The combined organic layers were dried over anhydrous Na_2SO_4 and concentrated *in vacuo*. The gummy residue was then triturated and washed with Et_2O, obtaining the pure compound in 43% yield (420 mg) as a white solid.

6-*O*-[(−)-D-Isoascorbic acid]-6′-*O*-[(−)-D-isoascorbic acid] Dodecanedioate. To a solution of (−)-D-isoascorbic acid (3.12 g, 17.74 mmol) and divinyl dodecanedioate (1.00 g, 3.44 mmol) in acetone (60 mL), 4 Å molecular sieves (5 g) and Novozym435 (700 mg) were added. The suspension was kept at 45 °C and shaken at 250 rpm for 16 h. The reaction was monitored by TLC [EtOAc/MeOH/H_2O (8:2:0.3)] and terminated by filtering off the enzyme. The filtrate was evaporated under reduced pressure, and the residue was dissolved in water and extracted by EtOAc (3 × 50 mL). The combined organic layers were dried over anhydrous Na_2SO_4 and concentrated in vacuo. The gummy residue was then triturated and washed with Et_2O, obtaining the pure compound in 49% yield (921 mg) as a white solid.

6-*O*-[(+)-L-Ascorbic acid]-vinyl Dodecanedioate. To a solution of (+)-L-ascorbic acid (600 mg, 3.40 mmol) and divinyl dodecanedioate (320 mg, 1.13 mmol) in acetone (40 mL), 4 Å molecular sieves (4 g) and Novozym435 (450 mg) were added. The suspension was kept at 45 °C and shaken at 250 rpm for 16 h. The reaction was monitored by TLC [EtOAc/MeOH/H_2O (8:2:0.3)] and terminated by filtering off the enzyme. The filtrate was evaporated under reduced pressure, and the residue was covered with petroleum ether (20 mL) and left at room temperature (r.t.) for 12 h without stirring. After decantation, the solid residue was purified by silica gel column chromatography [EtOAc/MeOH (95:5)], obtaining the pure compound in 78% yield (1.10 g).

6-*O*-[(+)-L-Ascorbic acid]-6′-*O*-[(−)-D-isoascorbic acid] Dodecanedioate. To a solution of 6-*O*-[(+)-L-ascorbic acid]-vinyl dodecanedioate (2.0 g, 4.83 mmol) and (−)-D-isoascorbic acid (850 mg, 4.83 mmol) in acetone (60 mL), 4 Å molecular sieves (5 g) and Novozym435 (450 mg) were added. The suspension was kept at 45 °C and shaken at 250 rpm for 16 h. The reaction was monitored by TLC [EtOAc/MeOH/H_2O (8:2:0.3)] and terminated by filtering off the enzyme. The filtrate was evaporated under reduced pressure, and the residue was then triturated and washed with Et_2O, obtaining the pure compound in 47% yield (1.24 g) as a white solid.

For the characterization of all synthesized products, see the Supporting Information.

Sample Preparation and Annhealing. All samples were prepared by weighing the proper amounts of the solid bolaamphiphile and water, with an accuracy of 0.01 mg. The vials were capped and sealed with Parafilm to prevent evaporation of water. The annhealing procedure was carried out by keeping the samples in a water bath at 70 °C, until a clear liquid was formed. The vials were then cooled to room temperature, which resulted in the formation of a white viscous paste (coagel), and put in a refrigerator at 4 °C for at least 30 min. The procedure was repeated three times, and the samples were finally stored in the refrigerator at 4 °C. All experiments were performed on freshly prepared samples, within 7 days from the preparation.

Differential Scanning Calorimetry. On the coagel samples, DSC experiments were carried out between −80 and 80 °C in order to investigate the coagel−micelles phase transition and to evaluate the different kinds of water in the samples. The experiments were done with a DSC-Q 2000 from TA Instruments (New Castle, PA, USA) equipped with the two-stage refrigerated cooling system RCS90. The samples were held in hermetically closed TZero aluminum pans.

The samples were transferred to the pans either in the form of solid paste (below the transition temperature), or in the liquid micellar state (preheated between 65° and 70 °C). The loaded pans were then closed immediately, reweighted, and placed in the autosampler of the DSC apparatus at room temperature. A constant nitrogen flow through the chamber was flushed with a flow rate of 50 mL/min. All samples were equilibrated at 4 °C for at least 30 min, simulating the storage in a fridge and to force the formation of the coagel phase. The samples were cooled and kept at −80 °C for 30 min and heated to 80 °C. The scanning rate was 2 °C/min for the

heating and 0.5 °C/min for the cooling step from 4 °C to −80 °C. The cooling/heating cycles were repeated twice for each sample.

In the case of the pure solids, the samples were equilibrated at 20 °C for 5 min and then heated to 120°, 140° or 160 °C, respectively.

The thermograms were analyzed with the Universal Analysis 2000 software (TA Instruments). The baseline used for the calculations was either of an integral type (for the melting of water) or a straight line (for the coagel−micelles phase transition).

Thermogravimetry. Thermogravimetric experiments were carried out with a SDT Q600 apparatus (TA Instruments), on the aqueous suspensions and on the freeze-dried solids. The proper amount of sample (1−5 mg) was placed in an open aluminum pan and measured against an empty reference while heating from room temperature to 400 °C for the solids, and from room temperature to 350 °C for the suspensions in water. The heating rate was 10 °C/min for all samples. A constant nitrogen flow of 100 mL/min was used.

X-ray Diffraction (XRD). Diffractograms were recorded by a powder Bruker D8 Advance Diffractometer (Bruker axs) using Bragg−Brentano geometry, λ = 1.54 Å (CuK_α). Experiments were carried out in the range $3° \leq 2\theta \leq 33°$, with a step size of 0.04°/s, a time/step of 1 s, and setting voltage and current at 40 kV and 40 mA, respectively. The peak assignment was made by applying Bragg's law.

Small-Angle X-ray Scattering. SAXS measurements were carried out with a Hecus SWAX camera (Kratky) equipped with a position-sensitive detector (OED 50M) containing 1024 channels of width 54 μm. CuK_α radiation of wavelength 1.542 Å was provided by a Seifert ID-3003 X-ray generator (sealed-tube type), operating at a maximum power of 2 kW. A 10 μm-thick nickel filter was used to remove the CuK_β radiation. The sample-to-detector distance was 275 mm. The volume between the sample and the detector was kept under vacuum during the measurements to minimize scattering from the air. The Kratky camera was calibrated using silver behenate, which is known to have a well-defined lamellar structure (d = 58.38 Å).[26] Scattering curves were monitored in a Q-range from 0.014 to 0.5 Å^{-1}.

The liquid samples were filled into a 1 mm quartz capillary using a syringe, whereas pastes were filled into a solid sample holder with thin Kapton windows, using a 1 mm stainless steel spacer and a Kalrez O-ring (perfluoroelastomer from Dupont). The temperature was controlled by a Peltier element, with an accuracy of ±0.1 °C. A temperature scan between 20 and 60 °C was performed using a temperature controller.

At the end of the experiment, the raw data were normalized to the actual acquisition time and to the operative power. All scattering curves were corrected for the empty cell contribution (kapton windows or quartz capillary) containing the solvent.

Due to smearing effects originating from the slit geometry, the curves had to be desmeared according to the procedure proposed by Lake.[27]

Fourier Transform Infrared Spectroscopy (FTIR). FTIR measurements were carried out using a Varian Golden Gate spectrometer (Varian, Inc., USA) with an ATR crystal, equipped with a measuring bridge and a stamp to press the sample on the diamond. The energy range investigated was between 4000 and 650 cm^{-1}, the resolution was set to 4 cm^{-1}, 32 single spectra were accumulated for the solids, and 64 were collected for the dispersions in D_2O. All measurements were carried out under ambient temperature and pressure. The spectra were background corrected.

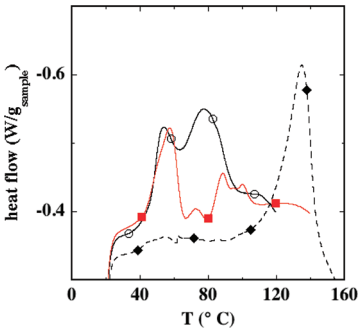

Figure 4. DSC profiles for freeze-dried pure solid bolaamphiphiles. DD: ○ (black solid line); DL: ■ (red solid line); LL: ♦ (black dotted line). Heating rate: 2 °C/min, endo up.

Thermoporometry. The procedure used to determine the pore size is based on the Gibbs−Duhem equation that relates the melting temperature of the confined water to the pore radius:[25]

$$\ln\left(\frac{T}{T_0}\right) \approx -\frac{\Delta T}{T_0} = -\frac{2V_l\gamma_{sl}}{r\Delta h_f} \quad (1)$$

Here, T is the equilibrium temperature, T_0 is the phase transition temperature (i.e., melting) in the bulk phase, Δh_f is the melting enthalpy change per unit mass, V_l is the molar volume of the liquid, γ_{sl} is the solid−liquid interfacial tension, and r_p and r are the radius of the pore and of the water droplet (see Figure 3). For a derivation of eq 1, see ref 25. Since $r_p = r \cos\theta$ (see Figure 3) and $V_l = M/\rho_l$, we obtain

$$\Delta T \approx \frac{2T_0\gamma_{sl}\cos\theta}{\rho_l r_p \Delta H_f} \quad (2)$$

where θ is the contact angle and ΔH_f is the molar melting enthalpy change.

However r_p is overestimated, because of the presence of nonfreezable liquid molecules along the walls of the pore. For very small pores, this effect is significant, and r_p can be replaced by $r_p - \delta$, where δ is the thickness of the permanent liquid layer that decreases the radius of the solid phase. Usually the relationship between r_p, ΔT, and δ has the following form:

$$r_p = \delta - \frac{a}{b + \Delta T} \quad (3)$$

the values of the empirical constants δ, a, and b were taken from the literature[25] as 1.12 nm, 19.082 nm·K, and 0.1207 K, respectively. These empirical constants imply spherical pores in the coagel.

While the pore radius is related to the temperature change obtained from the DSC profile (see eqs 2 and 3), the pore size distribution function is determined from the heat flow signal. In fact, the amount of heat absorbed or released by the sample is proportional to the amount of water that freezes or melts inside the pores, and the absolute heat flow dQ/dt can be used to calculate the pore size distribution dV/dr_p through the formula[25]

$$\frac{dV}{dr_p} = \frac{1}{\Delta H_f(T)\rho_{sol}(T)} \frac{dQ}{dt} \cdot \frac{dt}{d(\Delta T)} \cdot \frac{d(\Delta T)}{dr_p} \quad (4)$$

dx.doi.org/10.1021/jp204920y |J. Phys. Chem. B 2011, 115, 11638–11649

Table 1. Peak Temperatures (T, in °C) and Total Enthalpy Change (in kJ/mol$_{bola}$)

	DD		DL			LL
T (° C)	54°	78°	57°	73°	89°	100°	135°
ΔH_{tot} (kJ/mol)	35.7		22.5			47.9

where $d(\Delta T)/dt$ is the constant heating rate, $d(\Delta T)/dr_p$ is obtained by deriving eq 3, $\Delta H_f(T)$ is the temperature dependent molar enthalpy of fusion, and $\rho_{sol}(T)$ is the temperature-dependent density of the solid (for melting experiments).

RESULTS AND DISCUSSION

Synthesis. The chemical protocols for the preparation of "hybrid" nonsymmetrical compounds (such as DL in Figure 3) are quite troublesome and require protection/deprotection steps and a rigorous control of the reaction conditions. The structural complexity and inherent "fragility" of these molecules make them ideal substrates for a biocatalyzed approach, exploiting the regioselectivity of lipases and proteases suspended in organic solvents[28,29] for the direct coupling of "naked" sugar drivatives.

Different authors reported that activated dicarboxylates (i.e., divinyl adipate) are accepted by these enzymes as acyl donors,[30−34] and herein we show that indeed lipase regioselectivity can be efficiently exploited to link together ascorbic acid and its epimer.

In the following, we will first discuss the results of the pure solids and then of the aqueous dispersions of the bolaamphiphiles.

Pure Solids. *Differential Scanning Calorimetry and Thermogravimetry.* Figure 4 reports the DSC profiles for the solid bolaamphiphiles. LL shows one single endothermic peak (centered at 135 °C). DD and DL show a set of different endothermic peaks: at 54° and 78 °C for the former, and at about 57°, 73°, 89° and 100 °C for the latter.

The presence of more than one signal can be ascribed to a series of independent structural processes within the solid during the heating process, such as a rotational reordering of the head groups and/or a change in the order of packing of the chains and to the evaporation of some hydration water residues that were not removed by freeze-drying. Such reordering of the head groups does not occur with LL; instead, the polar groups interact consistently through intermolecular hydrogen bonding (HB). Conversely, the D-isoascorbic residues are involved in intramolecular HB, and therefore are more free to move. Interestingly, the two endothermic contributions in the DSC curve for DD are very close to the first two contributions for DL. This fact suggests that they are related to a structural reordering of the D-isoascorbic residues. In fact, it is known that in L-ascorbic acid, intermolecular HB is established by the carbonyl group in position 1 as the acceptor site.[13,35] Instead, the formation of intramolecular hydrogen bonds is inhibited in the same molecule, as the hydrogen atom in position C-4 points in the same direction. On the other hand, in the epimeric D-isoascorbic acid molecule, the position of the hydrogen in position C-4 is reversed. This implies that an intramolecular ($C_3OH\cdots O-C_5OH$) hydrogen bond can be established in D-heads. This feature holds for the parent acids and also for their bola derivatives, as only the hydroxyl group in position C-6 is involved in the ester linkage.

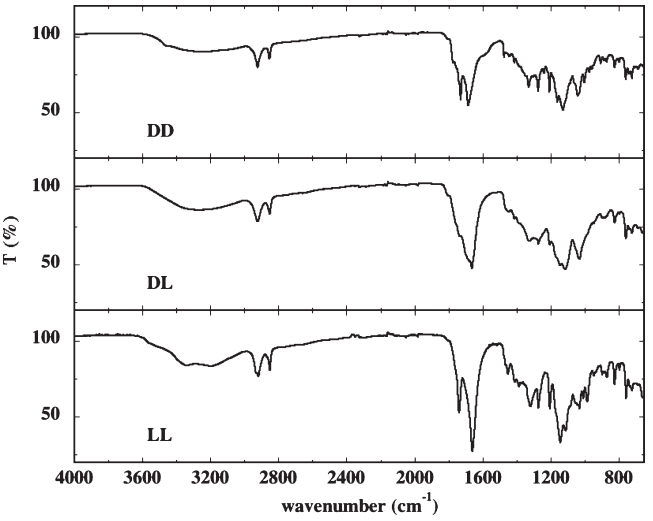

Figure 5. FTIR spectra of pure solid LL, DL, and DD bolaamphiphile.

For DD and DL, the phase transition starts at 40 °C and is stretched over a temperature range of almost 60 °C without any significant decomposition, as confirmed by thermogravimetric experiments. Thermogravimetric analysis (TGA) measurements show a 3% loss in weight, presumably due to the evaporation of hydration water. The enthalpy change and the temperatures for the phase transition of the solids are summarized in Table 1.

The highest value for ΔH_{tot} was reported for LL, confirming the presence of strong intermolecular hydrogen bonds between the headgroups, while DD and DL show a significantly lower transition enthalpy change, due to the weaker interactions between the polar heads.[13,14] These results suggest that the headgroup chirality and the inter/intramolecular hydrogen bonds dictate the phase behavior of these compounds in the solid state.

Studying the behavior of mixtures of L-ascorbyl-dodecanoate (L-ASC12) and D-isoascorbyl-dodecanoate (D-ASC12), we found that when L-ASC12 is the minor component in the solid mixture, the crystalline structure of the D-isoascorbic head is strongly perturbed. Conversely, when L-ASC12 is the main component, and D-ASC12 acts as an impurity, no crucial perturbation is induced in the crystalline packing of the L-ASC12 molecules.[14] The effect of the mutual structural influence of D-ASC12 and L-ASC12 in their mixture is useful to discuss the properties of the asymmetric DL bola molecule. In this case, the unfavored interaction between the D-isoascorbic and L-ascorbic headgroups belonging to two adjacent molecules results in a less pronounced crystallinity, a less-ordered chain packing, and therefore a lower transition ΔH.

TGA experiments (see Figure S1 in the Supporting Information) indicated that the freeze-dried solid samples heated between 20° and 400 °C released one molecule of water per bolaamphiphile molecule. These water molecules were not removed from the samples during the freeze-drying procedure.

Fourier Transform Infrared Spectroscopy. The FTIR spectra of the pure, freeze-dried solids are reported in Figure 5. In the O−H stretching region, between 3700 and 3000 cm^{-1}, DD shows two broad peaks centered at 3230 and 3066 cm^{-1}, and a narrow peak at 3454 cm^{-1}. In DL we recorded one single broad

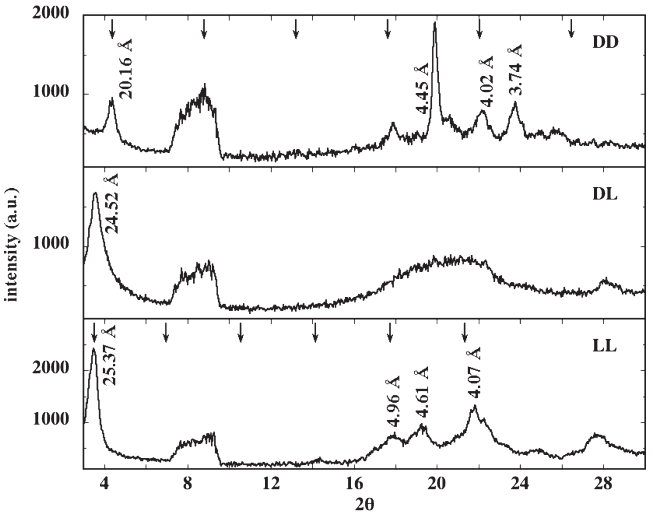

Figure 6. XRD profiles for pure freeze-dried solid DD, DL, and LL bolaamphiphile. The arrows indicate the calculated lamellar reflections according to the Bragg equation.

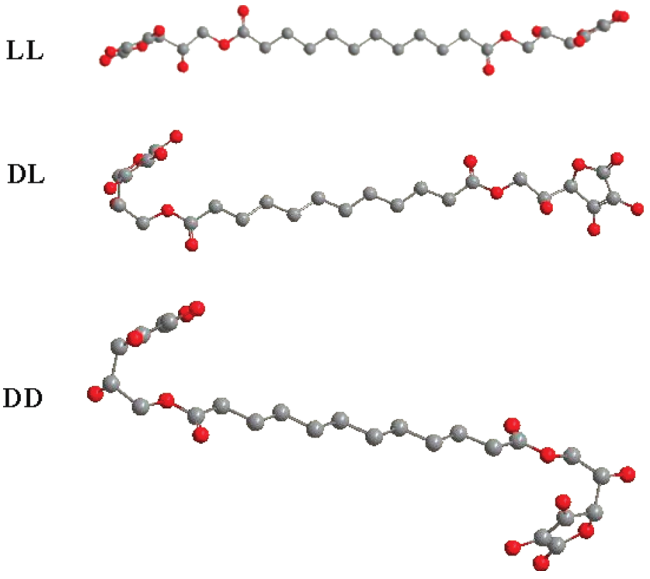

Figure 7. Proposed Corey–Pauling–Koltun (CPK) structures for LL, DL, and DD bolaamphiphiles. Gray, white, and red circles represent carbon, hydrogen, and oxygen atoms, respectively.

peak at 3263 cm^{-1}. The spectrum of LL shows a shoulder at 3540 cm^{-1}, a peak at 3340 cm^{-1}, and a broader peak at 3198 cm^{-1}.

The peaks reflect the stretching of the O–H groups in positions C-2, C-3, and C-5. With respect to DD, the peaks produced by LL are blue-shifted, indicating a stronger O–H bond and a less-pronounced HB. This finding confirms that the L-ascorbic acid groups preferentially establish intermolecular hydrogen bonds over a larger distance, while the D-isoascorbic residues are stabilized by intramolecular hydrogen bonds. In the case of intramolecular hydrogen bonds, the distance between the acceptor and the donor site is shorter, leading to a relatively stronger charge transfer. In the asymmetric DL bola, the average of the two effects brings about an overlap of those contributions and results in a broad signal, with no shoulders.

The C–H stretching region covers the range between 3000 and 2700 cm^{-1}. In this region of the spectrum, DD shows a peak at 2923 and a shoulder at 2957 cm^{-1}. This signal appears also for the DL sample, while for LL two overlapping peaks are resolved at 2930 and 2918 cm^{-1}. The second vibration is centered at 2850 cm^{-1} for DL and LL, and at 2854 cm^{-1} for DD. LL shows an additional shoulder at 2870 cm^{-1}. The CH_2 stretching modes, due to the aliphatic chain, appear between 3000 and 2800 cm^{-1}. The asymmetric mode produces the peaks centered between 2950 and 2900 cm^{-1}, and the symmetric modes are located between 2860 and 2840 cm^{-1}. Similar values were obtained for L-ASCn surfactants (single chain, single headgroup): 2919 and 2852 cm^{-1}, respectively. The small blue shift of the symmetric C–H stretching mode in DD may be due to a more ordered packing of the chains in the solid, as the XRD results confirm (see below).

The C=O and C=C stretching modes appear between 1800 and 1500 cm^{-1}, and are due to the C=O bond of the ester carbonyl, to the C=O bond of the lactone, and to the C=C bonds of the ascorbic ring. DD produces a main peak at 1729 cm^{-1}, with weaker peaks at 1738 and 1684 cm^{-1} and other shoulders. For LL, the first peak is broad and centered at 1738 cm^{-1}, while the second is red-shifted to 1660 cm^{-1}. In general, the peaks in DL are less intense and broader, and the spectrum shows the features of both DD and LL spectra, with a shoulder between 1730 and 1740 cm^{-1}, a peak at 1660, and a shoulder at 1685 cm^{-1}. The signal at 1660 cm^{-1} in LL and DL is assigned to a C=C vibration of the enediol group of the lactone ring. The blue shift to 1684 cm^{-1} for DD is presumably due to the tilt of the D-isoascorbic group toward the chain, resulting in a shorter and stronger C=C bond that appears at a higher wavenumber. For DD and LL, the peaks between 1738 cm^{-1} and 1729 cm^{-1} are found at the same wavenumber, but with different intensities. These signals are due to the vibrations of the carbonyl in the lactone ring and that of the ester bond.

Finally, the fingerprint region is comprised between 1500 and 650 cm^{-1}. Here a variety of C–H scissoring, wagging, twisting and deformation modes as well as O–H deformation, C–O–C, and other vibrations are detected. In particular, OH deformations are found at 1328 cm^{-1} (for DD), 1324 cm^{-1} (for DL) and 1319 cm^{-1} (for LL). The C=C bonds produce a signal at 1161 cm^{-1} (for DD), 1143 cm^{-1} (for DL) and 1142 cm^{-1} (for LL), and the same trends are followed as in the range between 1700 and 1600 cm^{-1}.

X-ray Diffractometry. The XRD profiles for the pure, freeze-dried solids are shown in Figure 6.

The first signal at low 2θ values corresponds to the length of the bolaamphiphile molecule with the aliphatic chains in the fully stretched *all-trans* conformation. The lengths are 20.16 Å for DD, 24.52 Å for DL, and 25.37 Å for LL. The value for LL agrees with the data reported in the literature.[24] Several signals are detected for DD and LL at 2θ larger than 15°, and correspond to different reflections of the packed chains.[36] In DL, a quite broad signal is observed between 14° and 25°, corresponding to a distance between 6.3 and 3.6 Å, and indicating an amorphous structure with a quite disordered packing of the chains.

In comparison to DD, a higher fluidity of the hydrocarbon chains in LL is suggested by the broadening of the signals in the short spacing region between 16° and 24°. Assuming that the first peak is the first-order reflection of a lamellar phase, the expected

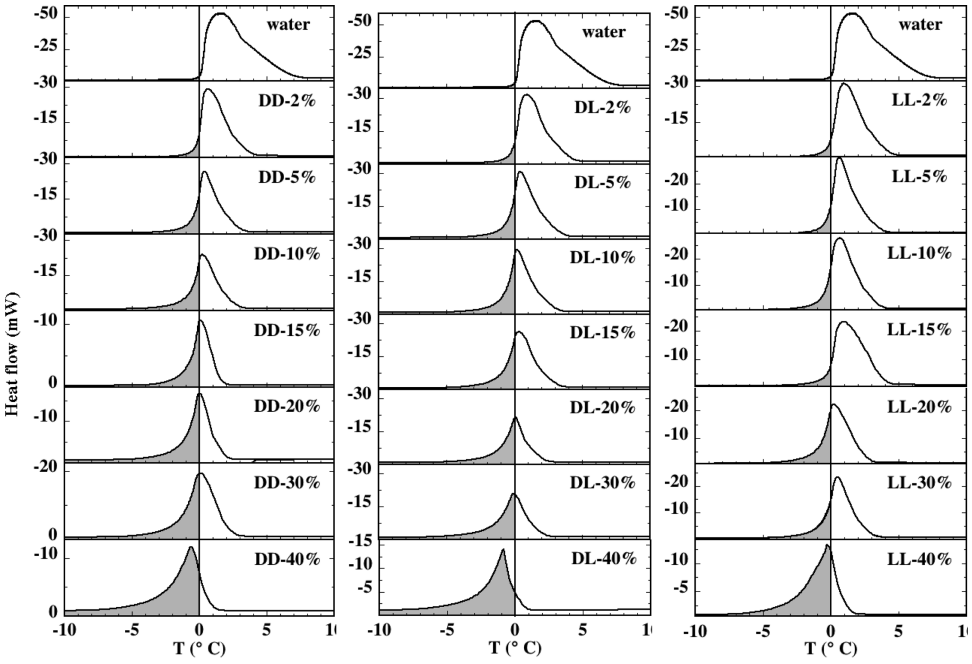

Figure 8. Melting endothermic profiles of freezing water for DD, DL, and LL coagels with bola concentrations ranging between 0 and 40% in water, between +10° and −10 °C. The gray regions (below 0 °C) refer to the bound freezing water. The white regions above 0 °C refer to bulk water. Heating scan: 2 °C/min; endo up.

higher reflections can be calculated according to the Bragg equation. The arrows in Figure 6 indicate the calculated *d* spacings (see Table S1, Supporting Information). In the case of the DD derivative, we found all the calculated reflections in the spectrum, meaning that the solid has a well-ordered lamellar structure, with an interlamellar distance of 20.16 Å in the crystalline state. In particular, the reflections at 4.45 Å, 4.02 Å, and 3.72 Å suggest a triclinic packing of the chains.[37] For the DL derivative, no distinct features for a lamellar ordering were found. The reflection between 15° and 25° is very broad, indicating a quite disordered packing. In the case of the LL bola, the lamellar ordering is not as pronounced as in DD. The peaks at 14.29°, 17.84°, and 24.87° correspond to the IV, V, and VII lamellar order. The signals due to the chain packing are observed at 4.96 Å, 4.60 Å, and 4.07 Å and suggest the presence of either a monoclinic or orthorhombic packing of the chains in the solid.[37]

Combining the structural results and the length of the molecules in their fully stretched conformation (DD < DL < LL), the molecular structures of the three bola derivatives can be depicted as illustrated in Figure 7.

According to this picture and to our previous findings,[24] the LL derivative forms lamellar layers in the solid state, the chains are fully stretched, and the headgroups lie perpendicularly to the planes formed by the chains. The short spacing suggests an orthorhombic or monoclinic packing of the surfactant.[37]

In the case of DL, no distinct feature for a rigid ordered chain packing was found in the short spacing region. As already mentioned, the tilt of the D-isoascorbic headgroups toward the chain, depicted in Figure 7, is more pronounced with respect to that of the L-ascorbic acid heads, and produces a shorter length. The same feature was found for L-ASC12 and D-ASC12.[14]

The extended length and the short spacing peaks of DD suggest a triclinic packing of the chains. According to Tanford's rule,[38] the length of the alipathic chain is about 12.7 Å, therefore the D-isoascorbic heads must be completely folded toward the hydrocarbon chain, resulting in a headgroup size of about 3.6 Å in the axial direction, much smaller than the size of the L-ascorbic group in LL.

Water Dispersions. *Differential Scanning Calorimetry: Water of Hydration.* The aqueous dispersions of the bolaamphiphiles exhibit a strong endothermic signal around 0 °C in the heating cycle, and the onset of the melting peak progressively shifts to lower temperatures as the concentration of the bola derivative is increased, as shown in Figure 8. In first approximation[39] the white area of the melting signal on the high temperature side of the vertical line (centered at 0 °C) is due to undisturbed or *bulk water*, while the gray region below 0 °C corresponds to what we define as *bound freezing water*.

As the concentration of the bolaamphiphile (*P*% w/w) increases (from top to bottom), the amount of bulk water decreases, while that of the bound freezing water increases. Moreover, the fraction of bound freezing water at $P = 40\%$ is larger for DD and DL with respect to LL. This is probably due to the strong disturbance of the dynamic structure of water induced by the D-isoascorbic heads,[15,16] reducing the amount of undisturbed bulk water in the sample. The experimental data and the calculated fraction of the different kinds of water are reported in Table S2 (Supporting Information).

From the measured melting enthalpy (ΔH_{exp}) and the enthalpy change of melting of pure water (ΔH_w, 333.79 J/g_{water}), the percentage of *strongly bound, nonfreezing water* (W_b) can be calculated as[24]

$$W_b = \left(1 - \frac{\Delta H_{exp}}{\Delta H_w}\right) \cdot 100 \qquad (5)$$

W_b quantifies the fraction of water that is strongly bound to the bolaamphiphiles' head groups, and therefore does not contribute to the endothermic signal around 0 °C. From W_b we can then calculate the number of strongly bound, nonfreezing water molecules per bolaamphiphile's head (N_b) as[24]

$$N_b = \frac{W_b}{100} \cdot \frac{100 - P}{2P} \cdot \frac{M_{bola}}{M_w} \quad (6)$$

Here P is the concentration of bolaamphiphile (in %, w/w) in the sample, M_{bola} is the molar mass of the surfactant (546.52 g/mol), and M_w is the molar mass of water. The factor "2" accounts for the presence of two hydrophilic headgroups in each surfactant molecule. At low surfactant concentration, N_b is certainly overestimated.[36] However, when the concentration of the bolaamphiphile is large (15% w/w or more), the value of N_b reaches a plateau of about 5 molecules of bound water per headgroup (see Figure 9), which is in good agreement with previous findings.[13,14,24,36]

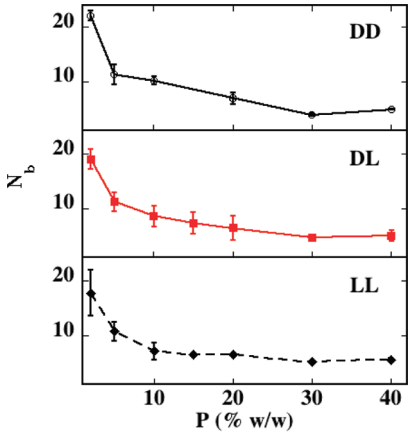

Figure 9. Number of strongly bound, nonfreezing water molecules (N_b) as a function of the bolaamphiphile concentration (P, in % w/w) for DD (○), DL (■), and LL (♦).

A careful perusal of the DSC profiles shows the presence of a small endothermic peak between −20° and −15 °C, just before the water melting process. This contribution was detected in all samples, and is part of the signal produced by the melting of a different kind of water, which we define as *bound freezing water*. The reason for the lowering of the melting point of water is based on various factors that can be explained by thermodynamic considerations (see the Materials and Methods section). Below the phase transition, when the sample is in the coagel state, a relevant number of small pores will form, and the water molecules confined in such microstructures possess a different melting behavior with respect to that of bulk water.[25,40,41] For this reason, the DSC cycles between −40° and 0 °C were analyzed in terms of thermoporometry, in order to determine the pore size distribution.[25,40−45]

DSC data need to be treated as illustrated in Figure 10. In particular, the procedure requires

i. the evaluation of ΔT as $T_{measured} - T_{onset}$
ii. the isolation of the endothermic signal
iii. a linear baseline correction
iv. the calculation of the enthalpy change of fusion (ΔH_f) and of the solid water density (ρ_{sol}) as a function of temperature as[25]

$$\Delta H_f(T) = 334.1 + 2.119\Delta T - 0.00783(\Delta T)^2 \quad (7)$$

$$\rho_{sol}(T) = 0.917(1.032 - 1.17 \times 10^{-4}T) \quad (8)$$

v. the calculation of the x-scale in units of mean radius (in nm) as

$$R = 1.12 - \frac{19.082}{0.1207 + \Delta T} \quad (9)$$

vi. from which we obtain the $d(\Delta T)/dR$ derivative:

$$\frac{d(\Delta T)}{dR} = \frac{19.082}{(1.12 - R)^2} \quad (10)$$

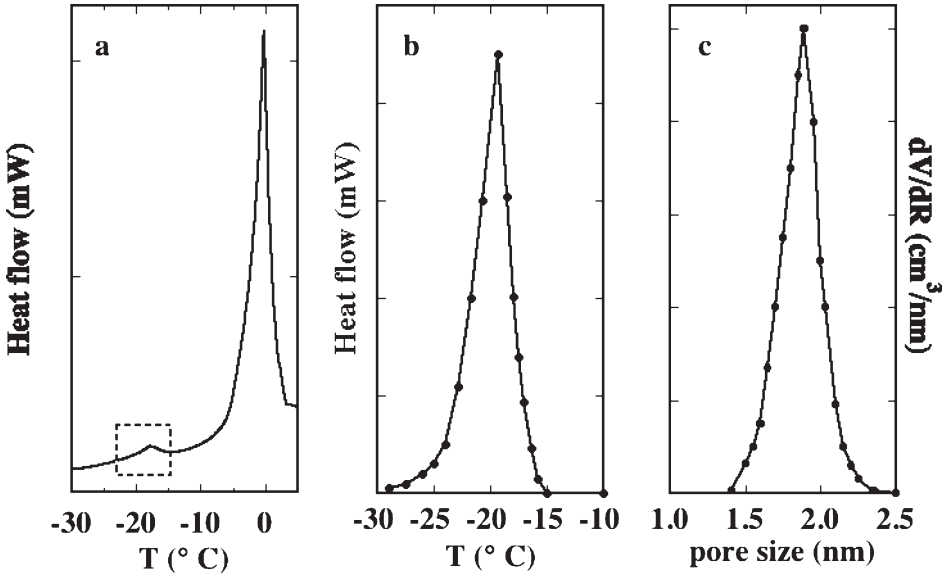

Figure 10. Data conversion from the DSC profile (a) to the baseline-corrected signal (b) and to the pore size distribution (c). Endo up.

dx.doi.org/10.1021/jp204920y |J. Phys. Chem. B 2011, 115, 11638–11649

Table 2. Mean Pore Radius (in nm) for DD, DL, and LL at Different Concentrations

P (%, w/w)	2	5	10	15	20	30	40
DD	2.0	1.9	1.9	2.1	1.9	2.2	2.0
DL	2.0	1.9	1.9	2.0	1.9		2.0
LL		2.2	2.3	3.2	2.0	3.5	2.9

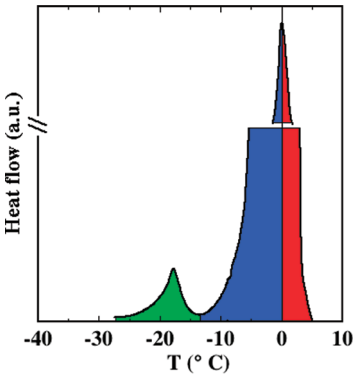

Figure 11. Melting ranges of different kinds of water. The picture was elaborated from the DSC profile of DD-30% w/w.

vii. the calculation of dV/dR using the baseline-corrected heat flow dQ/dt, knowing the constant heating rate $d(\Delta T)/dt$ as

$$\frac{dV}{dR} = \frac{1}{\Delta H_f(T)\rho_{sol}(T)} \frac{dQ}{dt} \frac{dt}{d(\Delta T)} \frac{d(\Delta T)}{dR} \qquad (11)$$

The endothermic signal around −20 °C is associated with a pore size of about 2.1 nm. The mean pore size values are reported in Table 2. LL shows higher values than DD and DL, which confirms the presence of larger aggregates in LL coagel samples[24] in the coagel, with larger interlayers of water where strongly bound solvent molecules are confined and reduce the melting point of water.

In summary, DSC measurements indicate the presence of four kinds of water, as illustrated in Figure 11:

(1) Undisturbed, bulk water molecules, that melt around 0 °C (red area in Figure 11).

(2) Non-freezing water molecules that are bound to the bolaamphiphiles' headgroups. This kind of water does not freeze in the investigated temperature range, and does not contribute to any signal related to melting processes. The number of non-freezing water molecules per headgroup (N_b) reaches a limit value of about 5 at high concentrations of surfactant.

(3) Freezing bound water in different environments:

(i) "intermediate" water confined between the amphiphile's lamellae, that starts melting at temperatures below 0 °C with an onset temperature that decreases with an increasing amount of the surfactant (blue area in Figure 11)

(ii) water confined in micropores (green area in Figure 11), that shows a melting endotherm around −20 °C. The average radius of the pores is about 2 nm for DD and DL, and slightly larger for LL.

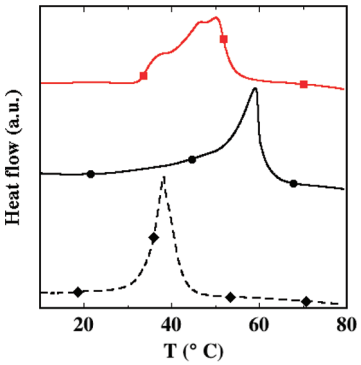

Figure 12. DSC thermograms for the coagel−liquid phase transition in 20% w/w aqueous dispersions of bolaamphiphiles: DD (●, black full line); DL (■, red full line); LL (♦, black dotted line). Heating rate: 2 °C/min, endo up.

Differential Scanning Calorimetry: Coagel-to-Micelle Phase Transition. Upon heating, the coagels undergo a phase transition and turn into liquid dispersions. The liquid dispersions contain micellar aggregates, as confirmed by SAXS experiments (see below). The endotherm peak shows up between 35° and 60 °C, depending on the particular bolaamphiphile as indicated in Figure 12.

The measured total ΔH_{trans} is given by different contributions:[24]

$$\Delta H_{trans} = \Delta H_{hydr} + \Delta H_{el} + \Delta H_{chain} \qquad (12)$$

here ΔH_{el} is the electrostatic endothermic contribution related to the release of H^+ ions from the acidic −OH groups in position 3 of the ascorbic ring, ΔH_{hydr} refers to the hydration of the protons and of the headgroups (exothermic contribution), and ΔH_{chain} (endothermic) reflects the reordering of the hydrophobic chains when the lamellar structures turns into the micellar aggregates.

The values of ΔH_{trans} are larger for DD than for LL and DL (see Table S3, Supporting Information). Since the three bolaamphiphiles bear the same hydrocarbons chain, ΔH_{chain} is assumed to be roughly independent of the stereochemistry of the heads. Instead, ΔH_{el} and ΔH_{hydr} depend on the hydration properties of the L- and D- head groups.

Previous studies have reported a lower acidity for D-isoascorbic acid headgroups in single-chain−single-head surfactants (D-ASCn) compared to the L-ascorbic acid derivatives (L-ASCn), because of the smaller headgroup cross-section that results from the intramolecular hydrogen bonds,[15,24] which implies a larger value of ΔH_{el} for the D-isoascorbic heads compared to the L-ascorbic groups, as the deprotonation process requires more energy because of thse spatial constraints. On the other hand, ΔH_{hydr} is greater for the D-isoascorbic residues, because the heads interact preferably through intramolecular hydrogen bonds, and therefore the hydration of the hydrophilic shell involves a larger endothermic contribution. In DL dispersions, the low ΔH_{trans} values are consistent with the fact that the interactions between D-isoascorbic and L-ascorbic heads of adjacent bola molecules are energetically unfavored, and therefore less energy is required to convert the coagel into the micellar dispersion upon heating.

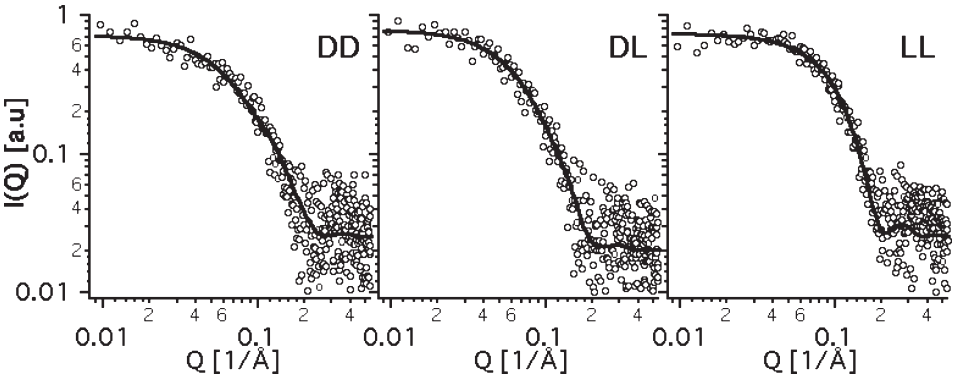

Figure 13. SAXS profiles for 5% aqueous dispersions of the bolaamphiphiles. From left to right: DD at 70 °C, DL at 55 °C, and LL at 60 °C. The data were fitted with a model function of cylinders.

Table 3. Fitting Parameters Obtained from the Guinier Analysis and Model Functions for Cylinders

	DD	DL	LL
temperature (° C)	70°	55°	60°
radius (R, Å)	14	17	18
length (L, Å)	79	74	35
polydispersity of R	0.02	0.06	0.01
bkg (cm^{-1})	0.025	0.02	0.025

Fourier Transform Infrared Spectroscopy. In order to investigate the vibrational modes of the bolaamphiphiles in the dispersed state, FTIR measurements have been carried out in D_2O at surfactant concentrations of 10% and 40% w/w. These sample compositions were selected for comparing the results to previous works on single-chained ascorbyl surfactants and because intermediate concentrations, between 10% and 40% w/w, did not show significant changes.

The broad bands observed in the spectra for the solid samples between 3600 and 3000 cm^{-1} (see Figure S2, Supporting Information) are shifted to higher wavenumbers for the dispersions in heavy water. The acidic protons (−OH groups in position 3 of the ring) are at least partially replaced by deuterium during the annhealing treatment, resulting in a higher vibrational frequency. The peaks are centered at 3411 for DD, 3419 for DL, and 3404 cm^{-1} for LL. With respect to the solid samples, the C−H vibrations are red-shifted from 2923 to 2916 cm^{-1} (asymmetric) and from 2854 to 2851 cm^{-1} (symmetric). In the case of DL, the position of the peaks is the same as that for the solid amphiphiles, while new peaks appear at 2954 and 2933 cm^{-1} for the asymmetric, and at 2870 cm^{-1} as part of the symmetric C−H stretching. These new signals are presumably due to the more ordered arrangement of the alkyl chains in the dispersions of the bolaamphiphiles. The C−H peak positions for LL are the same as in the solid samples. The asymmetric C−H stretching vibrations remain at 2930 and 2918 cm^{-1}, and the symmetric remain at 2850 and 2870 cm^{-1}.

In the 1900−1500 cm^{-1} region (Figure S3, Supporting Information), we found the most significant changes between the dispersions and the solids. For DD, the main peaks are red-shifted to 1709 and 1643 cm^{-1}. The peaks between 1800 and 1710 cm^{-1} are assigned to the different kinds of C═O vibrations, while the peaks below 1700 cm^{-1} result from the resonance of C═C bond vibration. Both contributions are red-shifted, indicating an elongation of the corresponding bonds in the aqueous dispersions. Both the C═O and the C═C bonds are affected by the formation of the dispersion state; in fact, they participate in the interactions between the amphiphiles and the solvent molecules. In DL, the shoulders found at 1737 and 1690 cm^{-1} in the solid phase form separated peaks in the dispersion state, while the peak at 1660 cm^{-1} disappears. In LL, the C═O peak remains centered at 1735 cm^{-1}, and only a slight red shift is recorded for the vibration of the C═C bond (from 1660 to 1646 cm^{-1}), indicating a partial weakening of this bond.

Small Angle X-ray Scattering. SAXS experiments were conducted on 5% w/w liquid samples above the transition temperature. The packing parameter $p = v_H/(l_H \cdot a_P)$ of the bolaamphiphiles ranges between 0.25 (for DD) and 0.31 (for LL), indicating that the surfactants should form nearly spherical or rod-like micellar aggregates in water.

SAXS experiments were performed at 70 °C (DD), 55 °C (DL), and at 60 °C (LL). The data were processed with a Guinier analysis to extract the radius of gyration of the aggregates present in solution. The Guinier $\ln(I \cdot Q)$ versus Q^2 plots are shown in Figure S4 (see Supporting Information), revealing a linear region characteristic of one-dimensional (1D) anisotropic scattering objects. For this reason, the $I(Q)$ versus Q profiles were fitted with a model function for cylinders to obtain the structural parameters (see Figure 13 and Table 3) associated with the aggregates. The fitting procedures were performed in IGOR Pro 6.2 using the SANS analysis 4.0 package,[46] available from NIST.[47]

The results confirm the presence of monodispersed elongated rod-like micellar structures in DD and DL dispersions, while LL forms shorter cylinders. The diameter of the rods comprises the length of the monomer (see Table S1) and two hydration layers (about 10 Å) for both the head groups. In the case of LL, the overall shape is very close to a spherical globule, which is consistent with the results already reported in a previous paper.[15]

■ CONCLUSIONS

Chirality is one of the most important structural features that determine and control the architecture and of supramolecular self-assemblies and the functionalities of biological complex systems. When the building block of the supramolecular aggregate is a surfactant that carries chiral head groups, then

the phase behavior of its aqueous dispersions is imparted by the stereochemistry and the different interactions established by the polar group. Therefore, the study of the properties of self-assembled nanostructures produced by chiral surfactants is important in order to determine the key factors that affect and control the peculiar features of supramolecular chiral structures.

Ascorbic acid amphiphilic derivatives possess a rigid structure of the lactone ring, and they carry several hydroxyl groups that establish inter- and intramolecular hydrogen bonds and a flexible hydrophobic side chain. Therefore these surfactants are a valid tool for investigating the effect of chirality on the physicochemical properties of the assemblies they produce.

In this contribution we have studied through DSC, TGA, FTIR, and SAXS the phase behavior in the solid and in the dispersed state of bolaamphiphilic molecules that bear L-ascorbic and/or D-isoascorbic acid moieties as head groups: the symmetric LL and DD, and the asymmetric DL isomers. All these compounds were prepared in good yield by using simple protocols that exploit enzymatic catalysis in organic solvents.

The results suggest that physicochemical properties of these bolaamphiphiles directly depend on the intra- and intermolecular hydrogen bonds (HB) that are set between the polar groups. In particular, L-ascorbic moieties preferentially establish intermolecular HB, while -isoascorbic residues form intramolecular HB.

Thermoporometry was used to analyze the DSC data on the aqueous dispersions of the surfactants, in order to assess the average size of the pores where some of the freezing bound water molecules remain confined.

In summary, the DSC measurements reveal the presence of four types of water: undisturbed bulk water molecules (that melt around 0 °C), non-freezing water molecules bound to the surfactants head groups (that do not freeze/melt), and freezing bound water. The latter kind comprises both the solvent molecules that are confined in the lamellar structure (that melt between −10° and 0 °C), and those that fill up the micropores and melt at about −20 °C.

■ ASSOCIATED CONTENT

Supporting Information. Additional details as described in the text. This information is available free of charge via the Internet at http://pubs.acs.org.

■ AUTHOR INFORMATION

Corresponding Author

*Fax: +39 (055) 457-3036. E-mail: pln@csgi.unifi.it. Internet: http://www.csgi.unifi.it/.

■ ACKNOWLEDGMENT

The authors acknowledge the Consorzio Interuniversitario per lo Sviluppo dei Sistemi a Grande Interfase (CSGI, Florence), the Ministero dell'Istruzione, dell'Università e della Ricerca (MIUR, Rome), and the CNR (target project "FUSINT") for partial financial support.

■ REFERENCES

(1) Purrello, R. *Nat. Mater.* **2003**, *2*, 216–217.
(2) Schulgasser, K.; Witztum, A. *J. Theor. Biol.* **2004**, *230*, 281–288.
(3) Selinger, J. V.; Spector, M. S.; Schnur, J. M. *J. Phys. Chem. B* **2001**, *105*, 7157–7169.
(4) Nyrkova, I. A.; Semenov, A. N.; Aggeli, A.; Boden, N. *Eur. Phys. J. B* **2000**, *17*, 481–497.
(5) Frankel, D. A.; O'Brien, D. F. *J. Am. Chem. Soc.* **1994**, *116*, 10057–10069.
(6) Lehn, J.-M. *Supramolecular Chemistry, Concepts and Perspectives*; VCH: Weinheim, Germany, 1995.
(7) Whitesides, G. M.; Simanek, E. E.; Mathias, J. P.; Seto, C. T.; Chin, D.; Mammen, M.; Gordon, D. M. *Acc. Chem. Res.* **1995**, *28*, 37–44.
(8) Nyrkova, I. A.; Semenov, A. N.; Aggeli, A.; Boden, N. *Eur. Phys. J. B* **2000**, *17*, 481–497.
(9) Cornelissen, J. J. L. M.; Rowan, A. E.; Nolte, R. J. M.; Sommerdijk, N. A. J. M. *Chem. Rev.* **2001**, *101*, 4039–4070.
(10) Terech, P.; Weiss, R. G. *Chem. Rev.* **1997**, *97*, 3133–3160.
(11) Bombelli, C.; Bernardini, C.; Elemento, G.; Mancini, G.; Sorrenti, A.; Villani, C. *J. Am. Chem. Soc.* **2008**, *130*, 2732–2733.
(12) Boyd, B. J.; Krodkiewska, I; Drummond, C. J.; Grieser, F. *Langmuir* **2002**, *18*, 597–601.
(13) Ambrosi, M.; Lo Nostro, P.; Fratini, E.; Giustini, L.; Ninham, B. W.; Baglioni, P. *J. Phys. Chem. B* **2009**, *113*, 1404–1412.
(14) Lo Nostro, P.; Ambrosi, M.; Ninham, B. W.; Baglioni, P. *J. Phys. Chem. B* **2009**, *113*, 8324–8331.
(15) Wang, Y.; Tominaga, Y. *J. Chem. Phys.* **1996**, *104*, 1–6.
(16) Umehara, T.; Tominaga, Y.; Hikida, A.; Mashimo, S. *J. Chem. Phys.* **1995**, *102*, 9474–9479.
(17) Mashimo, S.; Miura, N.; Umehara, T. *J. Chem. Phys.* **1992**, *97*, 6759–6765.
(18) Wang, Y.; Tominaga, Y. *J. Phys. Soc. Jpn.* **1993**, *62*, 4198–4201.
(19) Palma, S.; Manzo, R. H.; Allemandi, D.; Fratoni, L.; Lo Nostro, P. *Langmuir* **2002**, *18*, 9219–9224.
(20) Lo Nostro, P.; Ninham, B. W.; Fratoni, L.; Palma, S.; Manzo, R. H.; Allemandi, D.; Baglioni, P. *Langmuir* **2003**, *19*, 3222–3228.
(21) Kodama, M.; Seki, S. *Adv. Colloid Interface Sci.* **1991**, *35*, 1–30.
(22) Sperline, R. P. *Langmuir* **1997**, *13*, 3715–3726.
(23) Borsacchi, S.; Ambrosi, M.; Lo Nostro, P.; Geppi, M. *J. Phys. Chem. B* **2010**, *114*, 15872–15878.
(24) Ambrosi, M.; Fratini, E.; Alfredsson, V.; Ninham, B.; Giorgi, R.; Lo Nostro, P.; Baglioni, P. *J. Am. Chem. Soc.* **2006**, *128*, 7209–7214.
(25) Landry, M. *Thermochim. Acta* **2005**, *433*, 27–50.
(26) Blanton, T.; Huang, T. C.; Toraya, H.; Hubbard, C. R.; Robie, S. B.; Louer, D.; Gobel, H. E.; Will, G.; Gilles, R.; Raftery, T. *Powder Diffr.* **1995**, *10*, 91–95.
(27) Lake, J. A. *Acta Crystallogr.* **1967**, *23*, 191–194.
(28) Riva, S. Exploiting enzyme chemoselectivity and regioselectivity. In *Organic Synthesis with Enzymes in Non-aqueous Media*; Carrea, G., Riva, S., Eds.; Wiley VCH: Weinheim, Germany,2008, 145.
(29) Carrea, G.; Riva, S. *Angew. Chem., Int. Ed.* **2000**, *39*, 2226–2225.
(30) Khmelnitsky, Y. L.; Budde, C.; Arnold, J. M.; Usyatinsky, A.; Clark, D. S.; Dordick, J. S. *J. Am. Chem. Soc.* **1997**, *119*, 11554–11555.
(31) Wu, Q.; Xia, X.; Lin, X. *J. Mol. Catal. B: Enzym.* **2008**, *54*, 76–82.
(32) Xia, A.; Wu, Q.; Lin, X. *Enzyme Microb. Technol.* **2008**, *42*, 414–420.
(33) Quan, J.; Chen, Z.; Han, H.; Lin, X. *Bioorg. Med. Chem.* **2007**, *15*, 1741–1748.
(34) Magrone, P.; Cavallo, F.; Panzeri, W.; Passarella, D.; Riva, S. *Org. Biol. Chem.* **2010**, *8*, 5583–5590.
(35) Liu, H.; Xiang, B.; Qu, L. *J. Mol. Struct.* **2006**, *794*, 12–17.
(36) Ambrosi, M.; Lo Nostro, P.; Fratoni, L.; Dei, L.; Ninham, B.; Palma, S.; Manzo, R.; Allemandi, D.; Bagloni, P. *Phys. Chem. Chem. Phys.* **2004**, *6*, 1401–1407.
(37) Shimizu, T.; Masuda, M. *J. Am. Chem. Soc.* **1997**, *119*, 2812–2818.
(38) Tanford, C. *J. Phys. Chem.* **1972**, *76*, 3020–3024.
(39) Valéry, C.; Artzner, B.; Robert, B.; Gulick, T.; Keller, G.; Grabielle-Madelmont, C.; Torres, M.-L.; Cherif-Cheikh, R.; Paternostre, M. *Biophys. J.* **2004**, *86*, 2482–2501.

(40) Jähnert, S.; Vaca Chávez, F.; Schaumann, G. E.; Schreiber, A.; Schönhoff, M.; Findenegg, G. H. *Phys. Chem. Chem. Phys.* **2008**, *10*, 6039–6051.
(41) Morishige, K.; Kawano, K. *J. Chem. Phys.* **1999**, *110*, 4867–4872.
(42) Brun, M.; Lallemand, A.; Quinson, J.; Eyraud, C. *Thermochim. Acta* **1977**, *21*, 59–88.
(43) Iza, M.; Woerly, S.; Danumah, C.; Kaliaguine, S.; Bousmina, M. *Polymer* **2000**, *41*, 5885–5889.
(44) Ishikiriyama, K.; Todoki, M.; Motomura, K. *J. Colloid Interface Sci.* **1995**, *171*, 92–102.
(45) Ishikiriyama, K.; Todoki, T. *J. Colloid Interface Sci.* **1995**, *171*, 103–111.
(46) Kline, S. R. *J. Appl. Crystallogr.* **2006**, *39*, 895–900.
(47) SANS & USANS Analysis with IGOR Pro. http://www.ncnr.nist.gov/programs/sans/data/data_anal.html (accessed Sept 2011).